

Focal Depths and Mechanisms of Large Earthquakes on the Arctic Mid-Ocean Ridge System

JOHN P. JEMSEK,¹ ERIC A. BERGMAN, JOHN L. NABELEK,² and SEAN C. SOLOMON

Department of Earth, Atmospheric, and Planetary Sciences, Massachusetts Institute of Technology, Cambridge

As part of a global study of the source characteristics and tectonic implications of large earthquakes on mid-ocean ridges, we report on the focal depths and mechanisms of the six largest earthquakes that have occurred in the last 20 years on the Arctic mid-ocean ridge system. For each earthquake we invert the long-period *P* and *SH* waveforms to estimate the parameters of the best fitting point source, including seismic moment, centroid depth, double-couple source orientation, and source time function. Three of the earthquakes occurred on the oceanic spreading center in the Eurasian Basin, along ridge segments spreading at half rates of 4–6 mm/yr. These events have mechanisms very similar to those of ridge crest earthquakes on the Mid-Atlantic Ridge: almost pure normal faulting on planes that dip at approximately 45° and strike parallel to the rift axis, moments of $4\text{--}5 \times 10^{24}$ dyn cm, centroid depths of 1–2 km beneath the seafloor, and water depths (inferred from the predominant period of water column reverberations) appropriate to epicentral locations within the median valley. The remaining three earthquakes, also characterized by normal faulting, are associated with the continuation of the divergent plate boundary (2–3 mm/yr half rate) onto the continental shelf of the Laptev Sea, where the crust becomes transitional in nature. One of the largest known spreading center earthquakes (August 25, 1964, $M_0 = 1 \times 10^{26}$ dyn cm) occurred where the oceanic ridge intersects the outer edge of the continental slope. Waveform inversion for this event can resolve unilateral rupture from north to south (landward) along a fault at least 30 km in length. The preferred centroid depth is 5 km beneath the seafloor in crustal material with an unusually low shear velocity, but a centroid depth as great as 15 km cannot be ruled out. Two earthquakes beneath the continental shelf have significantly greater centroid depths (10–20 km) than mid-ocean ridge earthquakes, indicating a thicker brittle regime and a cooler thermal structure than are typical of oceanic spreading centers. The tectonic environment of these events is more representative of rifted continental lithosphere than of a mid-ocean ridge.

INTRODUCTION

The spatial distribution and source characteristics of earthquakes at mid-ocean ridges contribute important information on the tectonic processes accompanying the generation of new oceanic lithosphere. A particularly important quantity is earthquake focal depth because of the implications for determining the depth extent of brittle behavior at ridge crests [e.g., *Tapponnier and Francheteau, 1978*] and ultimately for understanding the local thermal structure and such controlling processes as shallow magma injection and cooling by hydrothermal circulation [*Lister, 1977*]. As part of a general and long-term study of earthquakes on mid-ocean ridges and their relationship to the spreading process, we are determining the focal depths and source characteristics (moment, double-couple orientation, source time function) of large earthquakes along the global mid-ocean ridge system from a formal inversion of long-period *P* and *SH* waveforms [*Nabelek, 1984*]. Results have been reported for earthquakes along the Mid-Atlantic Ridge by *Huang et al. [1986]* and on ridges in the Indian Ocean and Red Sea by *Huang and Solomon [1986]*. In this paper we present the source parameters of six of the largest earthquakes to have occurred in the past 20 years on the Arctic mid-ocean ridge and its continuation onto the continental shelf in the Laptev Sea.

The Arctic mid-ocean ridge is a particularly interesting target of study for two reasons. First, the ridge has one of the slowest spreading rates known, so that it offers an opportunity to look for differences in the maximum depth of faulting and other source parameters from earthquakes on faster spreading ridge systems. Second, the extension of the spreading center onto the continental margin permits an evaluation of the tectonic consequences of plate separation in a region which is transitional in character between an oceanic spreading center and an intracontinental rift.

TECTONIC SETTING

The Arctic mid-ocean ridge (Figure 1), also called the Nansen or Gakkel Ridge, is the northern continuation of the Mid-Atlantic Ridge and is the spreading center across which the Eurasian Basin has opened during the past 60 m.y. [*Pitman and Talwani, 1972; Vogt et al., 1979*]. The boundary between the North American and Eurasian plates continues landward through a broad, tectonically active belt in northeastern Asia [*Demenitskaya and Karasik, 1969; Grachev et al., 1970; Churkin, 1972*]. The present position of the pole of rotation for North American–Eurasian relative plate motion lies in northeastern Asia but is somewhat uncertain and depends on the interpretation of fault trends and earthquake slip vectors within the continental portion of the plate boundary zone [*Chapman and Solomon, 1976; Minister and Jordan, 1978; Savostin and Karasik, 1981; Cook et al., 1986*].

On the basis of identified magnetic anomalies [*Vogt et al., 1979*], the present half-spreading rate along the Arctic mid-ocean ridge is 3–6 mm/yr, in general agreement with the rate

¹ Also at MIT/WHOI Joint Program in Oceanography, Woods Hole Oceanographic Institution, Woods Hole, Massachusetts.

² Now at Lamont-Doherty Geological Observatory of Columbia University, Palisades, New York.

Copyright 1986 by the American Geophysical Union.

Paper number 6B6020.
0148-0227/86/006B-6020\$05.00

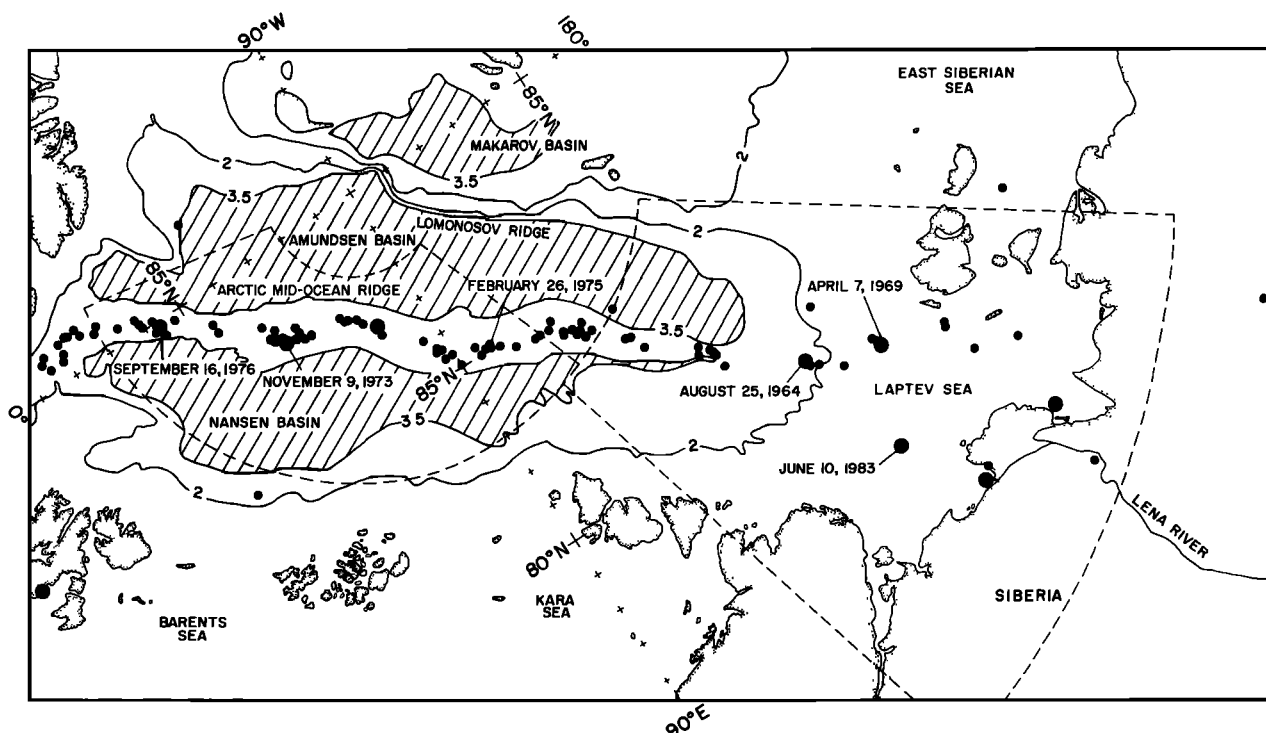


Fig. 1. Seismicity of the Arctic mid-ocean ridge system, with the locations indicated for the earthquakes studied in this paper. Earthquake epicenters are from the ISC for the years 1964–1982; larger symbols denote events with $m_b \geq 5.4$. The 2-km and 3.5-km bathymetric contours are also shown [Johnson *et al.*, 1979]; basins deeper than 3.5 km are shaded. The Eurasian Basin includes the Amundsen and Nansen basins as well as the intervening mid-ocean ridge. Polar stereographic projection.

of motion predicted from global plate velocity models [Minster and Jordan, 1978]. The spreading rate decreases along the ridge axis from west to east as the distance to the pole of rotation shortens. The extremely slow spreading rate is consistent with the rugged morphology and relief of the median valley; there are often well-developed inner and outer rift walls [Kristoffersen, 1982] bounding an inner valley floor that can exceed 5 km in depth.

Refraction experiments have verified that the Arctic mid-ocean ridge is underlain by oceanic crust of a thickness that may vary locally from 7 to as little as 2 km [Jackson *et al.*, 1982; Kristoffersen *et al.*, 1982; Duckworth *et al.*, 1982]. The seismic structure of the continental margin in the Laptev Sea, however, is less well known. On the basis of geophysical evidence, Grachev and Karasik [1974] suggested that a mid-ocean ridge spreading structure extends southward beneath the sediments of the continental slope and rise to at least latitude 76°N . Because of the small rates of separation between the North American and Eurasian plates and the large sediment flux discharged by the Lena River, the nature of spreading between about 80° and 76°N is more likely transitional in character between oceanic spreading and continental rifting [e.g., Moore, 1973; Einsele, 1985; Nicolas, 1985]. On the continental shelf, several graben systems define the locus of the plate boundary [Grachev, 1982]; refraction data indicate that extension is accompanied by crustal thinning [Kogan, 1974]. Sediment thicknesses are considerable across the continental margin; on the shelf, thicknesses range from 0.5 km on the structural highs to 8 km in the troughs [Ostenso, 1974].

EARTHQUAKE DATA SET

The seismicity of the Arctic has been the subject of a number of investigations [Sykes, 1965, 1967; Barazangi and Dorman, 1970; Tarr, 1970; Chapman and Solomon, 1976; Wetmiller and Forsyth, 1978; Savostin and Karasik, 1981; Fujita *et al.*, 1986]. In the Arctic Ocean, the North American–Eurasian plate boundary is well defined by a narrow zone of seismicity (Figure 1). At the outer edge of the Eurasian continental margin the seismic zone widens and becomes more diffuse. Almost all published source mechanisms for earthquakes on the Arctic mid-ocean ridge system indicate horizontal extension and normal faulting [Savostin and Karasik, 1981; Fujita *et al.*, 1986]. This predominance of normal faulting is generally in agreement with the lack of major transform faults on this ridge system, as indicated by the bathymetry and seismicity (Figure 1) as well as magnetic anomaly data [Vogt *et al.*, 1979]. Most mechanisms determined from P wave first motions are not well resolved, however, because of the generally small magnitude of Arctic events. In addition, the interpretation of first motions for mid-ocean ridge earthquakes is often complicated by apparently nonorthogonal nodal planes [Sykes, 1967; Solomon and Julian, 1974; Trehu *et al.*, 1981]. Reliable focal depths have not yet been reported in the literature for Arctic earthquakes.

Long-period body waves are large enough to use in waveform inversion studies for earthquakes in the Arctic with body wave magnitude m_b greater than or equal to about 5.3. We therefore examined records from stations of the

TABLE 1. Epicentral Data and Source Parameters for Earthquakes on the Arctic Mid-Ocean Ridge System

Date	Origin Time, UT	Latitude °N	Longitude °E	m_b	M_s	M_0^a 10^{24} dyn cm	Mechanism ^b	Centroid depth, ^c km	Location
Aug. 25, 1964	1347:19	78.15	126.65	6.2	6.5 ^d	121	346/47/271	5.1	continental slope
April 7, 1969	2026:30	76.55	130.86	5.4	5.5	1.9	314/48/254	10.2	continental shelf
Nov. 9, 1973	1342:41	86.05	32.8	5.4	5.1	5.0	45/63/255	1.3	Arctic mid-ocean ridge
Feb. 26, 1975	0448:53	84.98	98.5	5.3	5.6	4.9	314/41/254	1.9	Arctic mid-ocean ridge
Sept. 16, 1976	0326:55	84.30	0.9	5.4	5.5	4.7	30/51/258	1.9	Arctic mid-ocean ridge
June 10, 1983	0213:23	75.53	122.75	5.5	5.4	1.4	144/72/236	21.9	continental shelf

Epicentral and magnitude data are taken from the ISC.

^aUnits equivalent to 10^{17} N m.

^bFocal mechanism (strike, dip, slip, all in degrees) specified with the convention of *Aki and Richards* [1980].

^cDepth is relative to the seafloor.

^dMagnitude M from *Rothé* [1969].

World Wide Standard Seismograph Network (WWSSN) and Global Digital Seismic Network (GDSN) of all Arctic earthquakes with $m_b \geq 5.3$ in the bulletins of the International Seismological Centre (ISC) for the years 1964–1983. Excluding events within the land areas of the Soviet Union, we found six earthquakes suitable for body waveform inversion. The epicenters of these earthquakes are shown in Figure 1 and are listed in Table 1. Three occurred in the median valley of the Arctic mid-ocean ridge proper, two occurred on the continental shelf, and one occurred near the point where the mid-ocean ridge intersects the continental slope. Earthquake epicenters for large, well-located earthquakes in the Arctic should be accurate to within 10–20 km [Bungum and Husebye, 1977; Wetmiller and Forsyth, 1978].

Two additional events, one on the mid-ocean ridge and one on its extension onto the continental shelf, were deemed unsuitable for waveform modeling. A shelf earthquake on July 21, 1964 ($m_b = 5.4$), had extremely limited station coverage, and the records of a ridge crest earthquake on December 28, 1964 ($m_b = 5.6$), were obscured by the surface waves from a large earthquake which occurred in the Tonga region 50 min earlier.

WAVEFORM INVERSION PROCEDURE

For each of the earthquakes in Table 1 we determined the best fitting double-couple point source from an inversion of long-period P and SH waveforms recorded by WWSSN stations at teleseismic distances (30° – 80°). The inversion technique is that of *Nabelek* [1984]; our application follows the procedure described by *Bergman et al.* [1984]. The inversion yields the centroid depth and source time function as well as the double-couple orientation and scalar seismic moment. An independent estimate of the water depth in the epicentral region is also made by adjusting the thickness of the water layer in the source velocity model so as to yield synthetic waveforms that match the predominant period and phase of the water column reverberations in the later portions of the observed P waves.

A detailed investigation of depth resolution for shallow earthquakes along the Mid-Atlantic Ridge is described by *Huang et al.* [1986], who conclude that the uncertainty in the inferred centroid depth is typically ± 2 km. Two important considerations in the depth resolution are uncertainties in the source velocity structure and incomplete azimuthal coverage of the focal sphere [Huang, 1985]. Azimuthal coverage for large earthquakes in the Arctic region is generally good, with available waveform data typically spanning at least three quadrants of the focal spheres for both P and

SH waves. When signal-to-noise ratios or station coverage are less than optimal, *Huang et al.* [1986] found that a second minimum in the rms misfit versus centroid depth can develop at a depth immediately below the crust-mantle interface. For several reasons the shallow crustal solution was preferred for all Mid-Atlantic Ridge events, but the possibility of such secondary minima and their interpretation remain an important issue in source studies of very shallow earthquakes. For the three events on the Arctic mid-ocean ridge no significant local minimum was found at depths immediately below the Moho, and analysis of short-period P waveforms [Bergman and Solomon, 1985] confirm the shallow centroid depths determined from long-period waveform inversion. The adopted source velocity structure (Table 2) for the three mid-ocean ridge earthquakes is identical to that used by *Huang et al.* [1986], which facilitates a direct comparison of source parameters of ridge crest earthquakes in the Arctic and Atlantic. The source velocity structures assumed for the earthquakes beneath the continental slope and shelf are described separately for each event in the following section.

RESULTS OF WAVEFORM INVERSION

The best fitting source parameters obtained from body waveform inversion for the six earthquakes on the Arctic mid-ocean ridge system are presented in Table 1. The focal mechanism, source time function, and a comparison of observed and synthetic waveforms for each event are shown in a series of figures. The double-couple mechanism is specified by three angles in the order strike, dip, and slip,

TABLE 2. Source Structures Assumed for the Calculation of Synthetic Seismograms

Layer	V_p , km/s	V_s , km/s	Density, g/cm^3	Thickness, km
Arctic mid-ocean ridge				
Water	1.52	0.0	1.03	variable
Crust	6.4	3.7	2.9	6.0
Mantle	8.1	4.6	3.4	...
Laptev Sea				
continental slope				
Water	1.52	0.0	1.03	2.4
Sediment	2.5	1.3	2.1	2.0
Metasediment	5.2	2.7	2.6	4.0
Lower Crust	6.4	3.7	3.0	4.0
Mantle	7.9	4.3	3.3	...
Laptev Sea				
continental shelf				
Crust	6.0	3.46	2.5	...

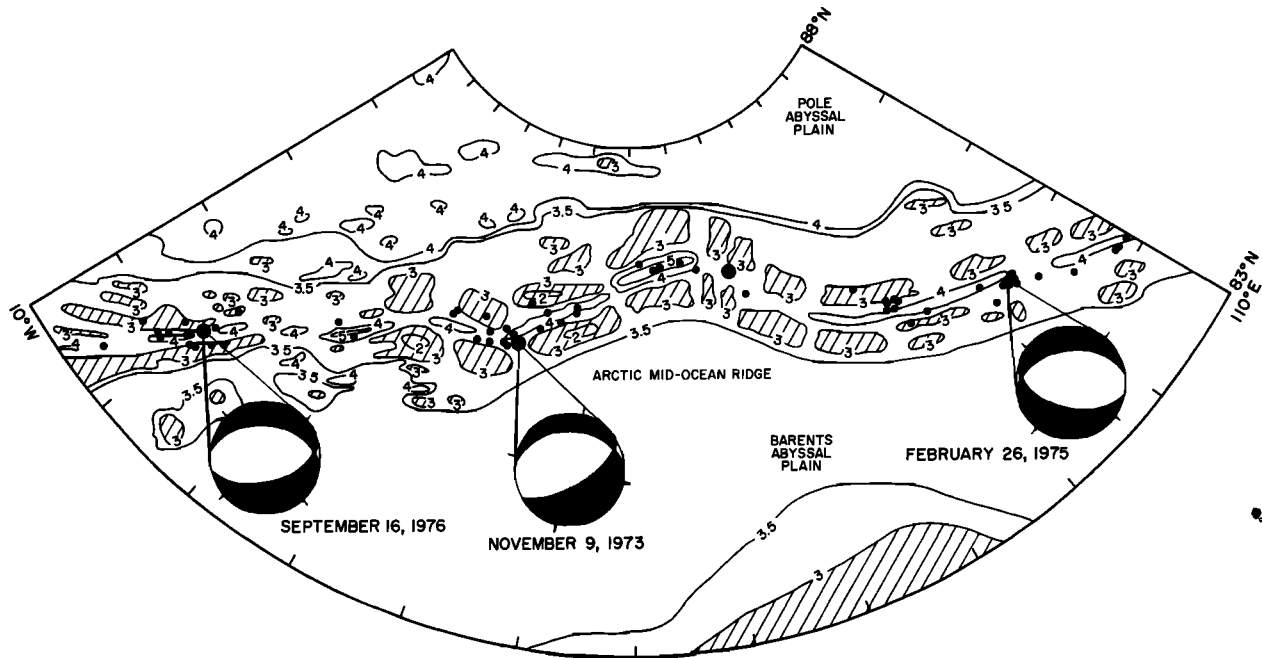


Fig. 2. Bathymetry and seismicity of the Arctic mid-ocean ridge near the epicenters of the earthquakes of September 16, 1976, November 9, 1973, and February 26, 1975. Bathymetric contours, in kilometers, are from Johnson *et al.* [1979]. Fault plane solutions are equal-area projections of the lower focal hemisphere; compressional quadrants are solid. Regions shallower than 3 km are shaded. See Figure 1 for further explanation.

using the convention of Aki and Richards [1980]. We consider the earthquakes in spatial order from west to east.

September 16, 1976

The earthquake of September 16, 1976, occurred in the Arctic mid-ocean ridge median valley (Figure 2). This event was the largest in a swarm of at least 11 events with $m_b \geq 4.5$. Station coverage is excellent for both P and SH waves (Figure 3), and a good overall fit to the observed waveforms is obtained with a normal-faulting mechanism (30/51/258) at a centroid depth of 1.9 km. There are some inconsistencies in the amount of dilatation observed in the P waveforms recorded at stations near one another; CAR has a much larger dilatation than SCP, for example. If the P waveform at CAR is not included in the inversion, a solution at a slightly shallower depth is possible. The seismic moment is 4.7×10^{24} dyn cm, and the duration of the source time function is about 3 s. The strike of the nodal planes is parallel to the local trend of the ridge axis. The epicenter of this event places it on the northwestern edge of the median valley (Figure 2), but the water depth of 4.1 km inferred from the reverberations in the P waveforms is consistent with a location nearer to the center of the median valley inner floor.

November 9, 1973

The ridge axis earthquake of November 9, 1973, was associated with two moderately large aftershocks ($m_b = 5.0$ and 5.1) and one foreshock ($m_b = 4.6$). A good fit to the observed P and SH waveforms is obtained with a shallow centroid depth (1.3 km below the seafloor) and a normal-faulting mechanism (45/63/255) with nodal planes subparallel to the local trend of the median valley (Figure 4). The seismic moment is 5.0×10^{24} dyn cm, and the source has a duration of about 5 s. The only P waveform which has a clear dilatational first motion is CAR; the small dilatational first

motions of the P waveforms predicted for WES and DUG by the best fitting point source are smaller than the background noise. The inversion solution reproduces the apparently compressional first motion of the P waveforms at COL, CHG, and QUE, all of which have high signal-to-noise ratios. The prominent reverberations in the water column are well matched in the synthetic P waveforms with a water depth of 4.1 km, which is very close to the depth of the inner floor of the median valley in the epicentral region (Figure 2). The SH waveform data are well distributed in azimuth and are generally well matched by the synthetic waveforms. A special effort was made to find a solution with an improved fit to the SH waveform at SHI, but without success.

February 26, 1975

The mid-ocean ridge earthquake of February 26, 1975 ($m_b = 5.3$), was accompanied by three small foreshocks ($m_b = 4.4$) and two aftershocks ($m_b = 4.3$ and 5.1). The P waveforms display clear dilatational first motions to the northeast and apparently compressional first motions to the southwest (Figure 5). A very good fit to the waveforms is obtained with a normal-faulting mechanism (314/41/254), with the steeper nodal plane dipping to the southwest. The centroid depth of the best fitting solution is 1.9 km below the seafloor. The seismic moment is 4.9×10^{24} dyn cm, and the total duration of rupture is about 3 s. SH wave coverage for this event is rather poor, which degrades the resolution of the double-couple mechanism somewhat. The strike of the nodal planes is close to the local trend of the median valley, and the water depth inferred from the dominant period of reverberations in the P waveforms (4.6 km) is close to the maximum local depth of the median valley (Figure 2). Savostin and Karasik [1981] reported a first-motion solution for this event (280/44/314) which is not compatible with the observed waveforms.

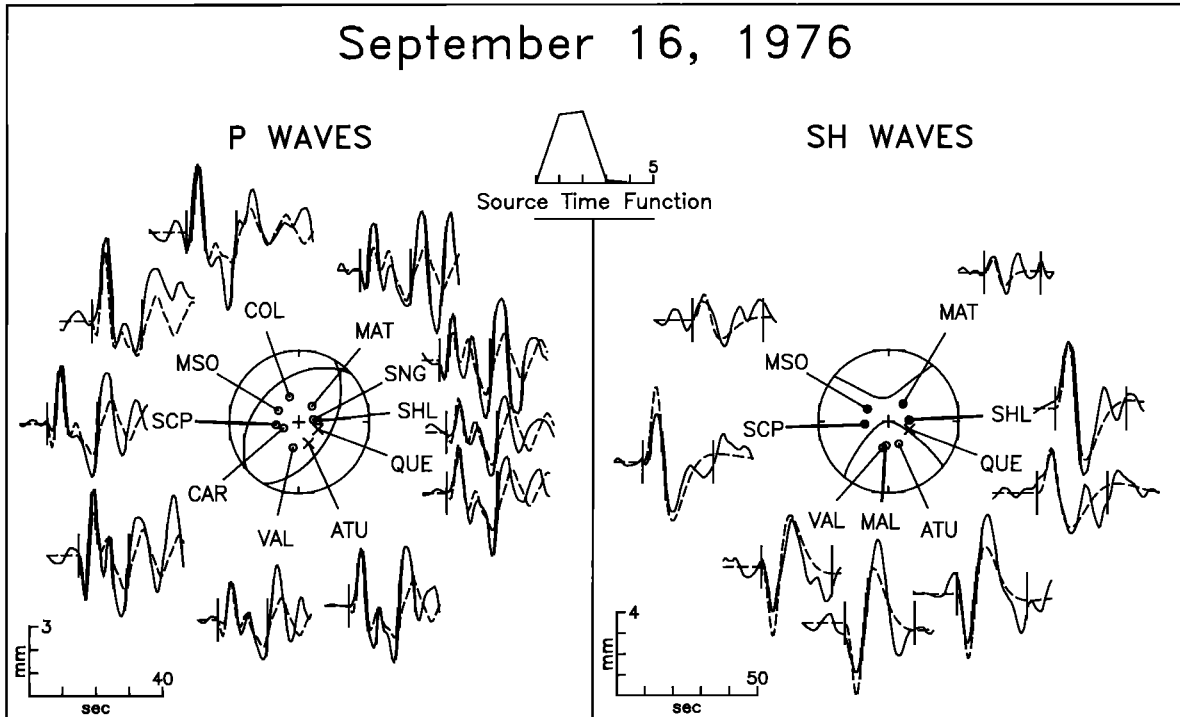


Fig. 3. Comparison of observed long-period *P* and *SH* waves (solid lines) from the September 16, 1976, earthquake with synthetic waveforms (dashed lines) generated for the best fitting source mechanism found in the body waveform inversion. *P* and *SH* radiation patterns are shown on the lower focal hemisphere (equal-area projection); station names and locations may be found in the work by *Poppe et al.* [1978]. The relative amplitudes of individual elements of the source time function are also shown. All amplitudes are normalized to a common epicentral distance of 40° and a common instrument gain of 3000; the amplitude scales correspond to the waveforms that would be observed on an original seismogram from such an instrument. The two vertical lines delimit the portion of each time series used in the inversion. The open circles denote dilatational first motion, solid circles denote compressional first motion, and crosses denote emergent arrivals. For the sign of *SH* wave amplitudes we follow the convention of *Aki and Richards* [1980].

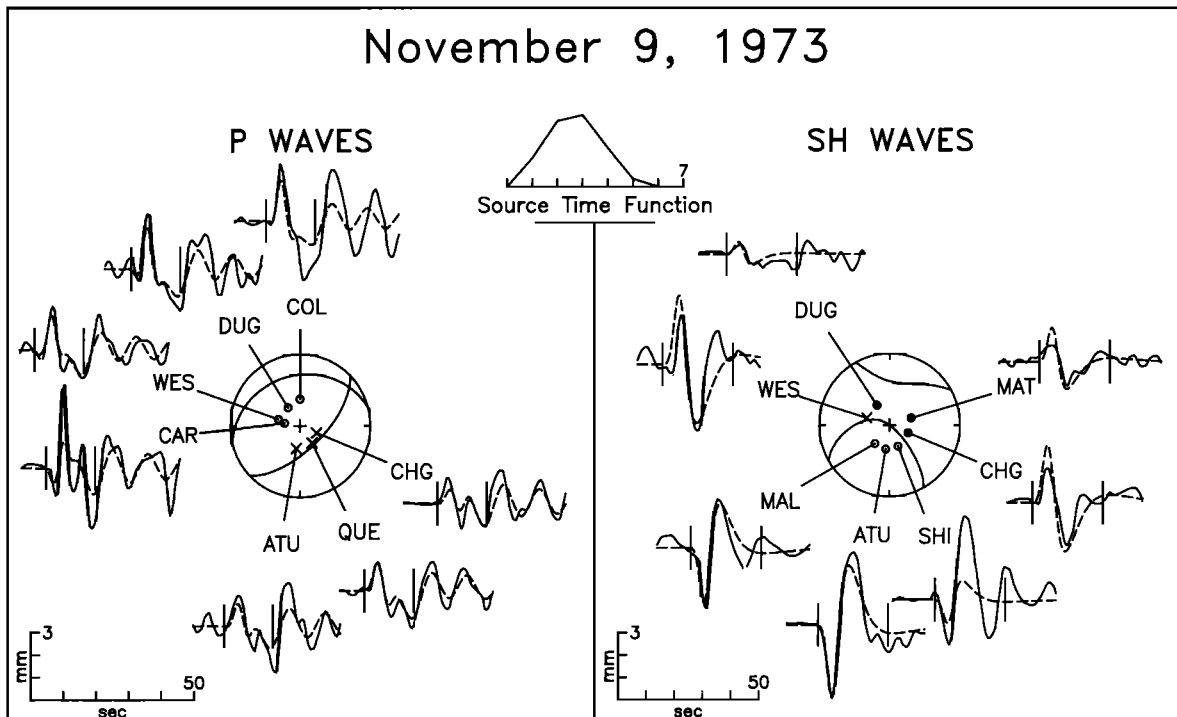


Fig. 4. Comparison of observed and synthetic *P* and *SH* waves for the earthquake of November 9, 1973. See Figure 3 for explanation of symbols.

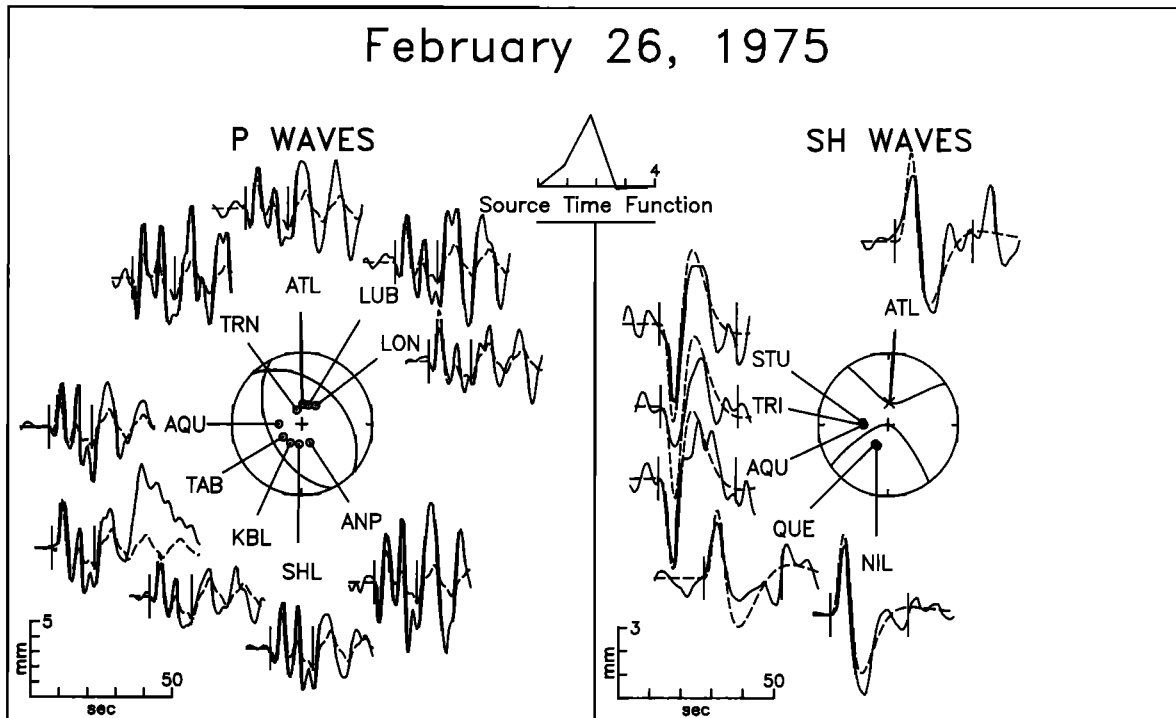


Fig. 5. Comparison of observed and synthetic P and SH waves for the earthquake of February 26, 1975. See Figure 3 for explanation of symbols.

August 25, 1964

The earthquake of August 25, 1964, occurred beneath the lower continental slope about 100 km seaward of the shelf break in the Laptev Sea (Figure 6). This earthquake is one of the largest to occur on the global mid-ocean ridge system. From long-period P wave first-motion data, Sykes [1967] found a normal-faulting mechanism (338/54/247) and strongly nonorthogonal nodal planes. Wyss [1970] estimated the moment as 3.7×10^{26} dyn cm from a surface wave amplitude measurement.

From the many P wave records available for this earthquake, we selected eight stations well distributed in azimuth and with high signal-to-noise ratios. The distribution of SH data is less ideal; seven of the eight stations used are at northern azimuths (Figure 7). Because of the unusually large signal-to-noise ratios, our normal procedure of weighting stations in inverse proportion to the noise [Bergman *et al.*, 1984] resulted in undue weighting of P waves relative to the SH waves. To restore balance to the weighting scheme in the inversion, we assumed equal (i.e., negligible) noise at all stations for both wave types.

The crustal velocity structure in the source region of the 1964 earthquake is poorly constrained because of both the unusual tectonic setting and the lack of published seismic data. Although a major topographic depression (the Sadko Trough) has been described on the lower margin [Churkin, 1972], the most recent bathymetric map of the area (Figure 6, from Johnson *et al.* [1979]) indicates a rather smooth continental slope and rise topography with a water depth of 2.4 km in the epicentral region. The absence of a bathymetric trough at the eastern extreme of the Arctic mid-ocean ridge attests to substantial deposition of sediment originating from the Lena River and the adjacent margins of the Eurasian basin. Grachev and Karasik [1974] have suggested that an

oceanic spreading center structure exists beneath the sediments to at least 100 km south of the 1964 epicenter.

As noted by others [Moore, 1973; Einsele, 1985; Nicolas, 1985], however, it is doubtful that normal oceanic crust can be generated when high sedimentation rates occur over an active oceanic spreading center. Instead, a thick metasedimentary layer consisting of intercalated sediment and basalt is likely to be present. Such structures have been inferred to be present in the Guaymas Basin in the Gulf of California [Saunders *et al.*, 1982] and the Galwood Knolls portion of the spreading center off the western coast of Canada [Clowes and Knize, 1979]. We have adopted a source structure for the epicentral region of the 1964 earthquake (Table 2) in isostatic balance with a median valley crustal section given by the assumed ocean ridge model in Table 2 (4 km of water and 6 km of crust). The P wave velocity and density structures are compatible with those reported by Fuis *et al.* [1984] for the upper crust of the Salton Trough.

For this structure there are two solutions, one with a centroid in the crust (5 km beneath the seafloor) and one with a centroid in the mantle (13 km). A double minimum in the curve for residual versus centroid depth was also observed by Huang *et al.*, [1986] for earthquakes on the Mid-Atlantic Ridge. Because of the uncertainty in source velocity structure, we also tested source models ranging from a half-space with velocities appropriate to continental crust to our standard oceanic structure with a thin sediment layer. The best fitting centroid depth depends on the details of the velocity structure, but the mantle solution is present for all structures tested in which the Moho is within about 10 km of the seafloor.

Solutions with centroid depths in the shallow crust provide a satisfactory fit to both P and SH waveforms only if a low shear velocity (less than 3 km/s) is present at depths of several kilometers beneath the seafloor. Shear velocities in

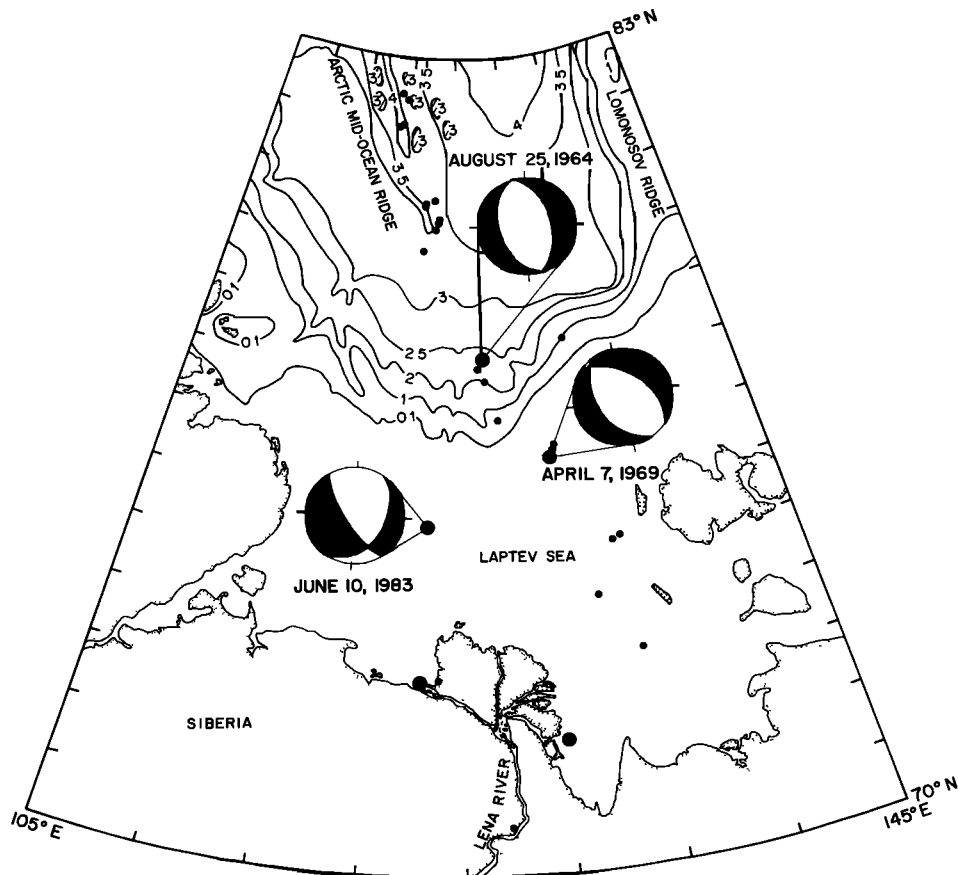


Fig. 6. Bathymetry and seismicity of the Laptev Sea region near the epicenters of the earthquakes of August 25, 1964, April 7, 1969, and June 10, 1983. In the Eurasian Basin, regions shallower than 3 km are shaded. See Figures 1 and 2 for further explanation.

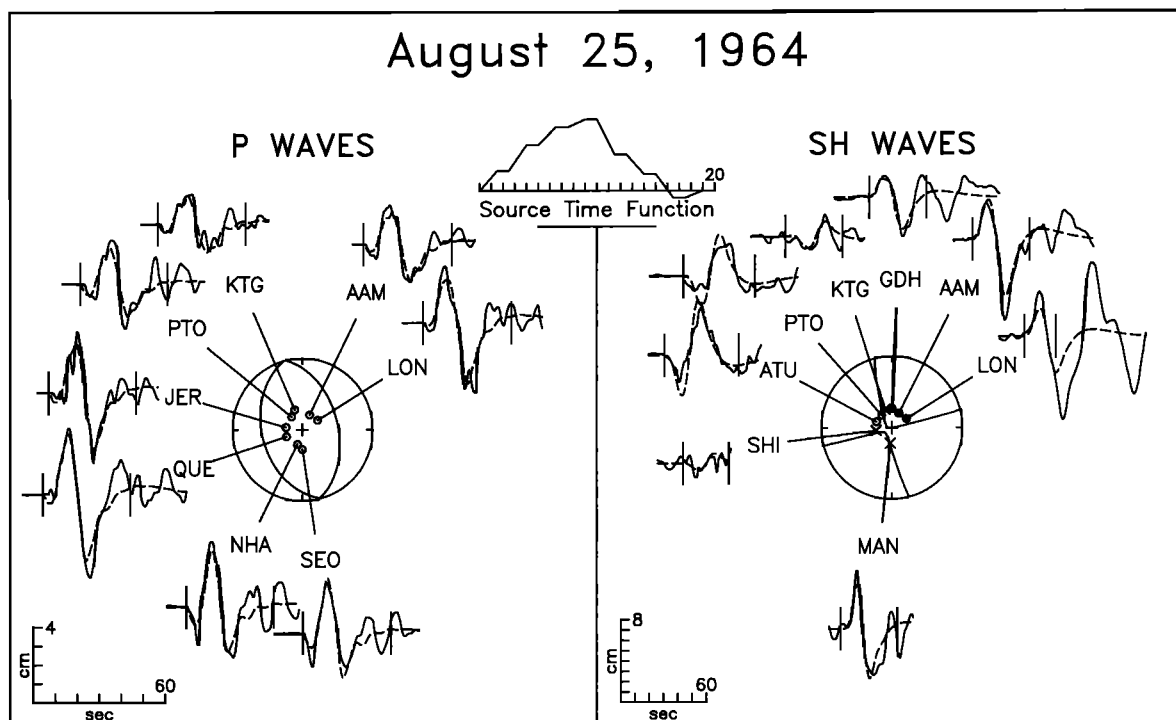


Fig. 7. Comparison of observed and synthetic *P* and *SH* waves for the earthquake of August 25, 1964. See Figure 3 for explanation of symbols.

the range 2.5–3.0 km/s are expected for upper basement rocks consisting of an intercalation of basalt and sediment [Hyndman, 1979; Hamilton, 1979]. The processes of fracturing and magma intrusion found at spreading centers would further increase the large-scale porosity as well as the V_p/V_s ratio. In contrast, velocity structures with a shear wave velocity at shallow depth near 3.5 km/s (typical of subbasement levels of continental crust or middle to lower oceanic crust) produce synthetic *SH* waves which are unacceptably large relative to the *P* waves.

This behavior for the shallow solution may be understood as follows. The ray parameter or takeoff angle used to calculate the synthetic waveform at each station is determined from the velocity at the centroid depth, and one of the consequences of a change in the assumed source velocity is that the average amplitude of the synthetic waveforms changes, reflecting a different sampling of the radiation pattern. For a normal-faulting mechanism the sense of this change in average amplitude is opposite for *P* and *SH* waves. For *P* waves a decrease in assumed velocity (takeoff angle) brings the rays closer to the center of the dilatational quadrant and slowly increases their predicted amplitudes, whereas for *SH* waves the rays approach the nodes of the radiation pattern, causing a rapid decrease in predicted amplitude (Figure 7). With compressional and shear velocities at shallow depth appropriate to lithified metasediments rather than the higher values generally assumed for other source settings, the amplitudes of the synthetic *P* waveforms are somewhat increased and those of the synthetic *SH* waves are significantly decreased (by approximately 50%), providing a better fit to the shapes and average amplitudes of all observed waveforms.

With the velocity structure as indicated in Table 2 for the earthquake of August 25, 1964, the shallow solution with a centroid 5 km beneath the seafloor, within the metasediment/basalt layer, provides the best fit to the waveforms (Figure 7). The mechanism represents nearly pure normal faulting (346/47/271), and the seismic moment is 1.2×10^{26} dyn cm. The waveform data (particularly the *SH* wave at MAN) indicate some source directivity, which we modelled as a horizontally propagating point source by expanding or contracting the source time function by a factor appropriate to the angle between the rupture direction and the ray takeoff direction [Ben-Menahem, 1962; Nabelek, 1985]. The best fit for horizontal rupture propagation along strike is from north to south, at an estimated average rupture velocity of 2 km/s. Any vertical component of rupture propagation is not resolved by the long-period body waveforms. The apparent source time function observed at a station in a direction perpendicular to the rupture vector is trapezoidal in shape and approximately 16 s in duration (Figure 7).

The second solution in the upper mantle (13 km centroid depth) has a residual error which is only slightly greater than that for the shallow solution. Except for centroid depth, the source parameters of the two solutions are nearly identical. The deeper solution has a somewhat shorter source time function (12 s) and slightly greater moment (1.35×10^{26} dyn cm). To investigate further the resolution of centroid depth for this earthquake, we performed a series of waveform inversions with the centroid depth held fixed at values between 2 and 18 km below the seafloor; all inversions were conducted with the source structure in Table 2. We then

employed a *t* test to determine the significance of differences in station residuals for the solution at different depths [Huang *et al.*, 1986]. At 90% confidence we can reject centroid depths shallower than 2 km or deeper than 15 km but no depth within these limits. At 75% confidence, acceptable centroid depths are 3–6 km, a range which includes only the shallow solution. We also note that for the upper mantle solution the alignment of synthetic and observed waveforms necessary to obtain the lowest residual results in some synthetic *P* waves starting earlier than the observed waveforms. This misfit in the first half cycle of motion contributes little to the total residual error, however. For these reasons, we favor the shallow solution as the best representation of the source for this earthquake. Nevertheless, we cannot reject a mantle-depth solution with high confidence.

It should be noted that in 1964, all WWSSN long-period seismometers had a pendulum period of 30 s. The response of these instruments reduces the resolution of source depth, compared with the resolution obtainable with the 15-s period instruments used at WWSSN stations after 1965. The resolution of centroid depth also suffers for shallow events with long source time functions because of the strong trade-off between these parameters.

There remain some high-frequency components to the observed waveforms that are unexplained by the inversion results (Figure 7). Their origin is probably related to source rupture complexities or heterogeneity in the source velocity structure. The water layer reverberations notable in the later part of the *P* waveforms are also not well reproduced in the synthetics. This is a consequence of the long, smooth source time function and provides additional evidence for unmodeled complexity in the source. Overall, however, the fit between observed and synthetic waveforms is exceptionally good, considering the size of the event and the simply parameterized model used in the inversion.

The fault plane solution with nonorthogonal nodal planes obtained by Sykes [1967] was constrained by apparently compressional first motions for two stations each in the NW and NE portions of the focal sphere. It is likely that in these records the impulsive reflected *P* wave half cycle instead of the emergent direct *P* wave onset was chosen in the Sykes [1967] solution. As demonstrated by Trehu *et al.* [1981], destructive interference between the direct arrival and surface reflections occurs for shallow events at certain takeoff angles, with the larger-amplitude surface reflections effectively masking the direct arrival. Nonorthogonality of the *P* nodal planes need not be invoked for this earthquake.

April 7, 1969

The April 7, 1969, earthquake occurred on the continental shelf of the Laptev Sea (Figure 6). Fault plane solutions showing predominantly normal faulting were reported by Chapman and Solomon [1976] (300/64/255) and by Savostin and Karasik [1981] (16/56/232). Because of the small size of the event ($m_b = 5.4$) and the poorly known velocity structure in the epicentral area, we conducted the waveform inversion with a source structure consisting simply of a halfspace with velocities appropriate for continental crust (Table 2). If a significant thickness of low-velocity sediments overlies crustal velocity material in the epicentral region, the centroid depth reported here (10 km) will be biased too deep. If the sediment thickness is as great as 8 km, tests indicate

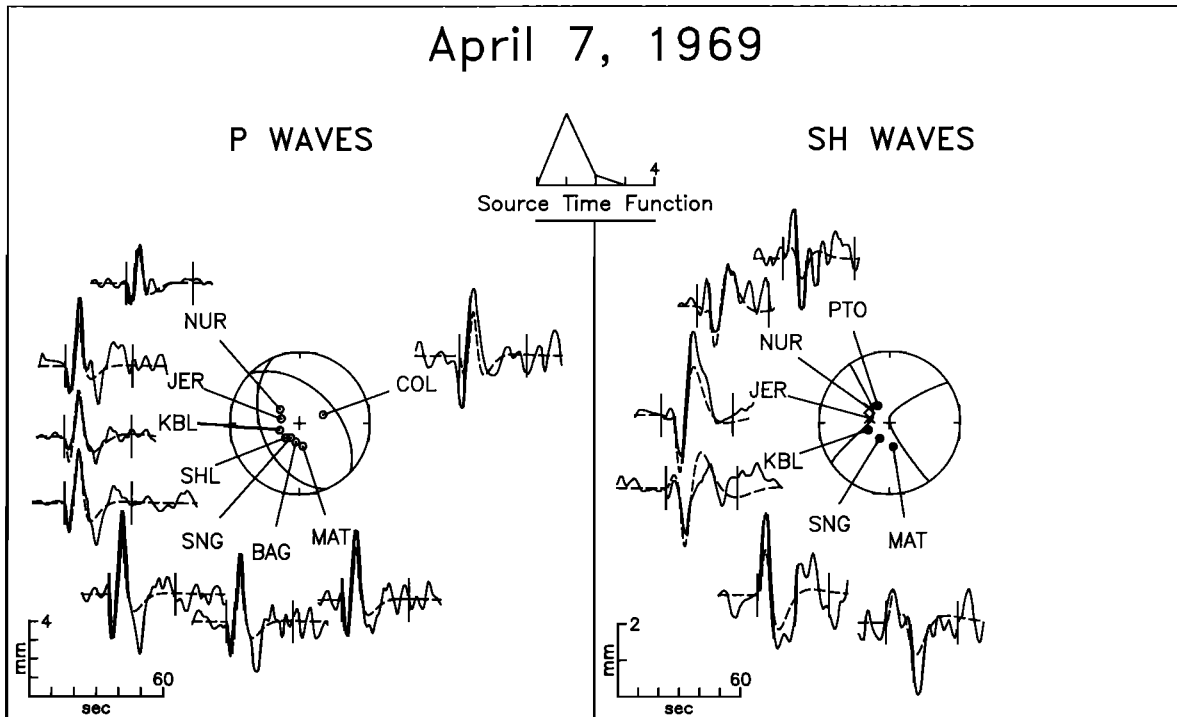


Fig. 8. Comparison of observed and synthetic P and SH waves for the earthquake of April 7, 1969. See Figure 3 for explanation of symbols.

that the centroid will lie just below the sediment layer, in the upper few kilometers of the basement.

Body waveform inversion for this event was hampered by poor station distribution (data span only 180° of azimuth) and the apparent complexity of the source (Figure 8). The source complexity can be seen in the P waveforms approximately 10 s after the initial dilatation; a pulse is clearly visible in the waveforms at JER and NUR. Though a multiple event is indicated, we were unable to resolve the source parameters of a second source because of the poor station distribution and rather poor quality of the SH waveforms. The solution shown in Figure 8 is for the single point source which best fits the long-period P and SH waveforms: a normal-faulting mechanism (314/48/254) at a centroid depth of 10.2 km. This mechanism is similar to that reported by Chapman and Solomon [1976], but the solution reported by Savostin and Karasik [1981] is not compatible with the body waveform data. The moment is 1.9×10^{24} dyn cm, and the source time function is about 2 s in duration. The uncertainties of these source parameters are somewhat greater than normal because of the unmodeled complexity of the waveforms.

June 10, 1983

The June 10, 1983, earthquake occurred on the continental shelf of the Laptev Sea, on the western edge of a several-hundred-kilometer-wide band of seismicity marking the extension of the Arctic mid-ocean ridge system onto the Eurasian continent (Figure 6). The epicenter is near the intersection of two graben systems, striking at azimuths of 142° and 44° , noted by Grachev [1982]. Because little is known about the velocity structure in this region, we performed the inversion with a continental crustal halfspace source model (Table 2). Water depth is less than 50 m in the epicentral region. A good fit to the observed P and SH waveforms (Figure 9) is obtained with a predominantly

normal-faulting mechanism (144/72/236), a source time function 3 s in duration, and a centroid depth of 21.9 km, making this the deepest event in this study. It is also the smallest ($M_0 = 1.4 \times 10^{24}$ dyn cm). If the crust in this region is thinner than 22 km, placing the centroid in the mantle, the centroid depth would be even greater. If a significantly thick layer of low-velocity sediments is present in the source region, however, the centroid depth would be less than 22 km. The potential error in centroid depth from uncertainties in the assumed velocity structure probably does not exceed 3 km.

The double-couple mechanism reported here is quite similar to the centroid moment tensor solution of Dziewonski *et al.* [1983] (142/59/242), but our data require a steeper dip for the southwest-dipping nodal plane. Dziewonski and coworkers, however, report a shallower centroid depth (12 km) and larger moment (3.6×10^{24} dyn cm) than we obtain. The WWSSN instrument response provides much better depth resolution for small events than the GDSN data, which as used by Dziewonski and coworkers are low-pass filtered at 45-s period. An overestimate of the seismic moment is a consequence of underestimating the centroid depth because of the predicted destructive interference between direct and surface-reflected phases.

The nodal plane striking at 144° is parallel to the strike of the southeast-trending graben system indicated by Grachev [1982], and the sense of slip is consistent with the southwestern side being down-dropped. The large component of strike slip motion in the mechanism may reflect structural complexities or heterogeneities in the stress field in the vicinity of the intersection of the two graben systems.

DISCUSSION

The source characteristics of the earthquakes of this study are quite similar. All show normal faulting with nodal planes dipping between 30° and 60° and (with the exception of the

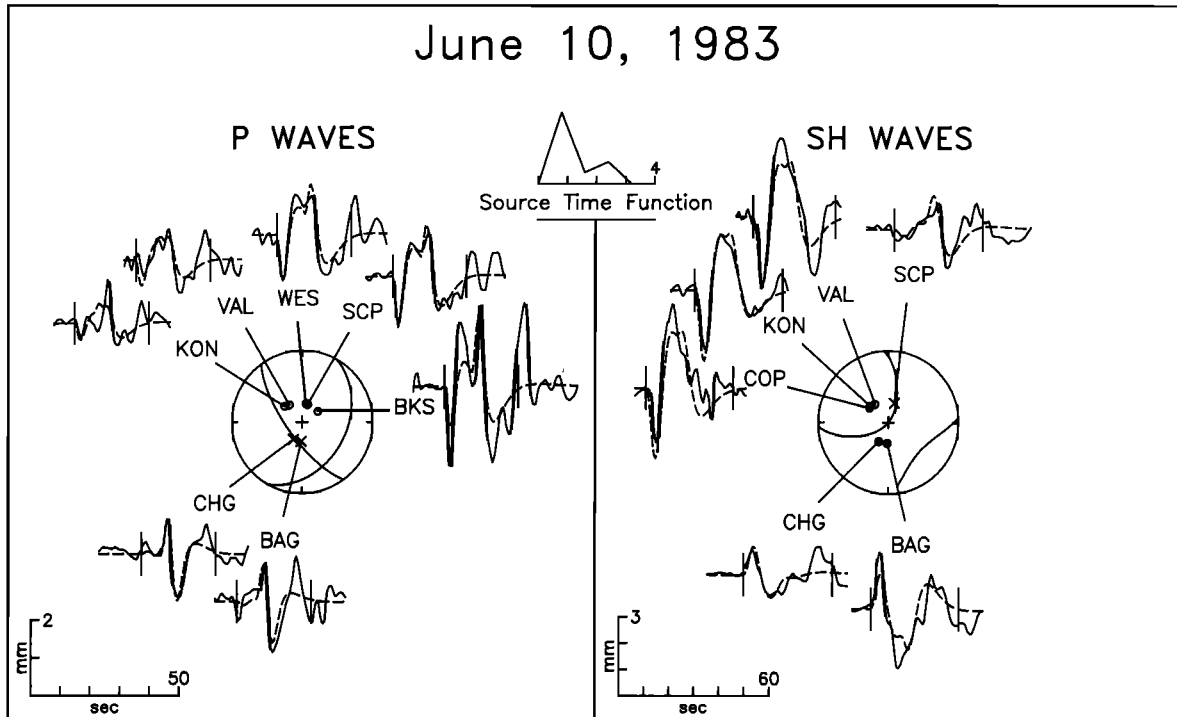


Fig. 9. Comparison of observed and synthetic P and SH waves for the earthquake of June 10, 1983. See Figure 3 for explanation of symbols.

1983 event) nearly pure dip-slip motion. The nodal planes of the mid-ocean ridge events strike approximately parallel to the ridge axis, and the T axes are aligned with the spreading direction (Figure 2). Since sediments obscure the basement topography of the Laptev Sea region, it is possible that the shelf and slope earthquakes could be associated with near-ridge tectonics [e.g., Bergman and Solomon, 1984] as opposed to plate boundary faulting. The horizontal projections of the slip vectors (Figure 6), however, are generally parallel to the direction of relative plate motion [Minster and Jordan, 1978; Savostin and Karasik, 1981], which suggests that the Laptev Sea events occur along the same divergent plate boundary as do the Arctic mid-ocean ridge earthquakes. Except for the earthquake of August 25, 1964, the seismic moments span a narrow range ($1.4\text{--}5 \times 10^{24}$ dyn cm), and the source time functions are of generally similar (2–5 s) duration.

From the centroid depth, the source time function, and the seismic moment we may obtain estimates of fault dimensions, average slip, and average stress drop for these earthquakes. For the two small and relatively deep shelf events (April 1969 and June 1983) we assumed a circular fault model [e.g., Ebel *et al.*, 1978], while for the very shallow Arctic mid-ocean ridge events a more appropriate model is a rectangular fault with unilateral rupture propagation and slip extending from the seafloor to twice the depth of the centroid [e.g., Huang *et al.*, 1986]. A bilateral rupture model for the ridge events will reduce the estimated slip and stress drop by factors of 2. The fault areas of the five smallest earthquakes in this study range from 35 to 70 km²; ratios of length to width for the mid-ocean ridge faults range from 1.5 to 4 (3 to 8 for bilateral rupture). The average slip on these faults varies from 10 to 35 cm, and the estimated stress drops lie between 10 and 30 bars (10–15 bars if the ridge axis earthquakes experienced bilateral rupture). Overall, these values

are within the ranges reported by Huang *et al.* [1986] for Mid-Atlantic Ridge earthquakes.

The August 25, 1964, earthquake had a seismic moment 2 orders of magnitude greater than the other events of this study and consequently a larger fault area and average slip. To estimate source dimensions, slip, and stress drop, we assume that the shallow solution (5 km below the seafloor) is correct. If, as for the mid-ocean ridge earthquakes, we assume further that slip occurred on a rectangular fault extending from the surface to a depth of twice the centroid depth, then faulting extended to 10 km depth. Directivity effects in the P waveforms indicate rupture from north to south on a fault 30–40 km in length. These source dimensions imply a ratio of fault length to width of about 2 or 3 and a fault area of 400–600 km². The stress drop is approximately 20 bars, comparable to estimates obtained for other earthquakes on the Mid-Atlantic Ridge and Arctic mid-ocean ridge system. The average fault slip (accounting for the lesser shear modulus than for normal oceanic crust) is about 1 m.

The tectonic interpretation of the 1964 event depends critically on the centroid depth relative to the local velocity structure. The high sedimentation rates likely in the region as well as the high V_p/V_s ratio indicated at the source for the shallow crustal solution suggest that the centroid is in a metasedimentary crustal layer. That the centroid lies within what is likely to be a mechanically weak layer is not as improbable as it may seem at first glance. If rupture initiates in crystalline basement rock and propagates upward through the thick metasedimentary and sedimentary layers to the seafloor, then the centroid can readily occupy a position within the metasedimentary/sedimentary sequence. With the crustal velocity model assumed (Table 2), a centroid depth of 5 km implies that faulting extended through most of the competent lower crust. If the centroid of this event is

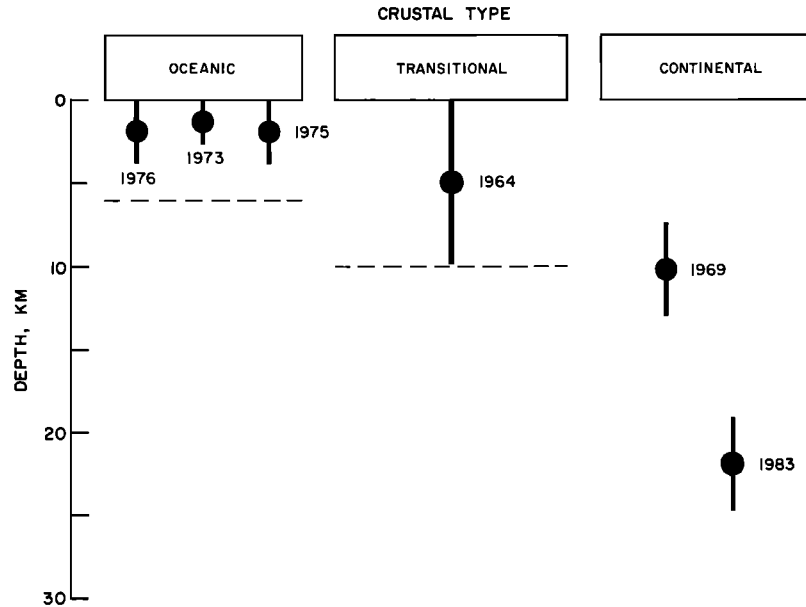


Fig. 10. Centroid depth as a function of geologic setting for the earthquakes of this study. Depths are relative to the top of the crust (Table 1). The base of the oceanic and transitional crust as assumed in the inversions is indicated by a dashed line; the continental crust is taken to be a simple halfspace (see Table 2). Vertical bars indicate the approximate vertical extent of faulting and are given by twice the centroid depth for the ocean ridge and 1964 events and by twice the inferred radius of the equivalent circular fault model for the shelf events (see text).

actually at a depth of 10–15 km, the maximum depth of faulting could be as great as 20 km. In young oceanic lithosphere, centroid depths of intraplate earthquakes do not exceed the depth of an isotherm near 800°C [Bergman and Solomon, 1984]. Centroid depths as great as 15 km are not observed for events in lithosphere less than about 8 m.y. old. An upper mantle depth for the August 1964 earthquake would therefore be an anomaly, suggesting that the upper mantle in the epicentral region is much cooler than would be expected for an active oceanic spreading center.

We have compared the tectonic setting to the centroid depths obtained by waveform inversion in Figure 10. The site of the 1964 event is viewed as transitional between the oceanic crust of the Arctic mid-ocean ridge and the rifted continental crust of the Laptev shelf. The ridge events are associated with spreading half rates of 4–6 mm/yr. The most striking feature of Figure 10 is that the shelf events occur at a much greater depth than the ridge events. Such a pronounced difference in centroid depth reflects differences in the thermal structure and associated mechanical properties of the oceanic and continental segments of the Arctic mid-ocean ridge system. It should be noted that because of the extremely shallow centroid depths of the ridge earthquakes, adoption of a source structure with a thinner crustal layer [Jackson *et al.*, 1982] would not have altered our results.

The centroid depths of the mid-ocean ridge events are similar to those of Mid-Atlantic Ridge earthquakes [Huang *et al.*, 1986]. No difference in the depth extent of median valley faulting is apparent despite the fact that half spreading rates in the North Atlantic (8–18 mm/yr) are greater than those in the Eurasian Basin by a factor of 2 or more. This is somewhat surprising since the maximum size of ridge axis earthquakes is greater on a slow spreading ridge than on a fast spreading ridge, presumably the result of a cooler thermal structure at lower spreading rates [Isacks *et al.*, 1968]. Of course, the thickness of the seismogenic layer is

likely to be locally time dependent along any given ridge axis segment, and three earthquakes may be too few to gauge the maximum depth extent of seismic faulting in this region. Further, the 1964 event, if interpreted as an ocean ridge earthquake, may be an indicator of the size of earthquakes that can occur on well-cooled segments of slow spreading ridge systems.

Estimates of the water depth in the epicentral region of the Arctic mid-ocean ridge earthquakes have been obtained by matching the water column reverberations in the synthetic and observed *P* waveforms. For these events, faulting occurs in the inner valley floor where water depths are greater than 4 km (Figure 2). As with large earthquakes on the Mid-Atlantic Ridge [Huang *et al.*, 1986], we can exclude the possibility that these earthquakes occurred in the rift mountains. Thus, on both ridge systems the largest ridge earthquakes occur where the brittle layer is probably thinnest. These observations support the hypothesis that lithospheric necking [Tapponnier and Francheteau, 1978] is a major deformation mechanism contributing to the formation of the median valley.

The centroid depths and inferred fault widths of the mid-ocean ridge earthquakes in the Arctic as well as along the Mid-Atlantic Ridge suggest that seismogenic faulting is primarily restricted to the upper portions of the oceanic crust. This result is consistent with structural observations of the Bay of Islands ophiolite complex which show that brittle fracture is maintained in the ophiolite units equivalent to oceanic layer 2 but that this fracturing gradually decreases in its pervasiveness with depth until it merges with laterally discontinuous foliated zones in the upper gabbroic section [Casey *et al.*, 1981]. Dike rotations observed in ophiolites [e.g., Varga and Moores, 1985], mylonitically deformed gabbros from the Mid-Atlantic Ridge [Karson and Dick, 1983], and shallow magnetic inclinations measured in North Atlantic Deep Sea Drilling Project holes [Verosub and

Moore, 1981] are consistent with substantial tilting of crustal blocks (by either simple block tilting or listric normal faulting) in the innermost median valley, with such blocks bounded below by a zone of ductile deformation. Strength envelopes constructed for slow spreading ridges support such a rheologic stratification [Tapponnier and Francheteau, 1978]. The vertical distribution of strength and the consequent geometry of faults accommodating ongoing extension is undoubtedly a function of time since the last major injection of crustal magma along a given ridge axis section [e.g., Harper, 1985].

As may be expected for rifting continental margins, the thick sediment cover complicates the tectonic interpretation of the earthquakes on the Laptev Sea continental shelf. The centroid depths of these events are in the range of focal depths observed in other continental extensional regimes; focal depths in such regions are generally less than 15 km, but some activity often extends to 20–30 km depth [Chen and Molnar, 1983; Shudofsky, 1985]. In comparison to the Arctic mid-ocean ridge the Laptev shelf has a broader zone of seismicity and a seismogenic layer that is several times thicker. These characteristics are interrelated: Because the extension is accommodated across a broad zone, the lithospheric thinning in the Laptev Sea is much less than along the mid-ocean ridge axis [e.g., McKenzie, 1978; Lachenbruch et al., 1985]. The lesser rate of opening in the Laptev Sea region also contributes to a generally cooler thermal regime, but this effect is probably of secondary importance.

Another distinction between mid-ocean ridge earthquakes and continental rift earthquakes that is demonstrated by the events studied here is the temporal behavior of local seismicity associated with each event. All the ridge events are members of distinct earthquake sequences, with the September 16, 1976, earthquake occurring in a swarm sequence of a type commonly observed on mid-ocean ridges [Sykes, 1970]. The shelf events and the large 1964 event are not accompanied by any teleseismically observed foreshocks or aftershocks. Earthquake swarms are generally attributed to heterogeneities in material properties and stress distribution in the region of the fault zone [e.g., Sykes, 1970]. The source dimensions of typical ridge axis faults could be an important factor in causing swarm activity. The anomalously thin faults may lead to an increased influence of typical fault asperities on the rupture process. Stress redistribution on a long, thin fault may lead to unusual stress concentrations near fault edges that trigger further events nearby. More accurate location of hypocenters of ridge axis earthquake sequences should aid in understanding the mechanisms of swarm behavior.

CONCLUSIONS

We have determined the centroid depths and focal mechanisms for the six largest earthquakes to have occurred on the Arctic mid-ocean ridge system in the last two decades. All events have normal faulting mechanisms and T axes that are generally horizontal and approximately parallel to the direction of relative motion between the North American and Eurasian plates. Three earthquakes on the Arctic mid-ocean ridge have centroid depths of 1–2 km and epicenters within the inner floor of the median valley. These characteristics are identical to earthquakes along the Mid-Atlantic Ridge [Huang et al., 1986], despite the significantly slower spreading rate in the Arctic. The shelf events occur at

centroid depths of 10–20 km. We infer that the rifting continental shelf has a considerably thicker brittle layer than does a mid-ocean ridge, a consequence of the reduced rates of opening and a much wider zone across which extensional strain is accommodated. The August 25, 1964, event occurred in crust transitional in character between ocean and continent, probably at shallow depth in a layer with a high V_p/V_s ratio which we interpret as metasediments. A centroid depth in the upper mantle, however, at a depth of 10–15 km below the seafloor, cannot be rejected with high confidence. Although the event occurred in an atypical setting, the large seismic moment (10^{26} dyn cm) may indicate the maximum size of a normal faulting earthquake on a slow spreading ocean ridge system.

Acknowledgments. We thank Paul Huang for helpful discussions, Kazuya Fujita for preprints of papers in advance of publication, and Jan Nattier-Barbaro for assistance in manuscript preparation. We also thank James Jackson and Joe Engeln for constructive comments on the manuscript. This research was supported by the National Science Foundation under grant EAR-8416192. Woods Hole Oceanographic Institution contribution 6283.

REFERENCES

- Aki, K., and P. G. Richards, *Quantitative Seismology: Theory and Methods*, vol. 1, p. 114, W. H. Freeman, San Francisco, Calif., 1980.
- Barazangi, M., and J. Dorman, Seismicity map of the Arctic compiled from ESSA, Coast and Geodetic Survey, epicenter data, January 1961 through September 1969, *Bull. Seismol. Soc. Am.*, **60**, 1741–1743, 1970.
- Ben-Menahem, A., Radiation of seismic body waves from a finite moving source in the earth, *J. Geophys. Res.*, **67**, 345–350, 1962.
- Bergman, E. A., and S. C. Solomon, Source mechanisms of earthquakes near mid-ocean ridges from body waveform inversion: Implications for the early evolution of oceanic lithosphere, *J. Geophys. Res.*, **89**, 11,415–11,441, 1984.
- Bergman, E. A., and S. C. Solomon, Broad-band and short-period body waveform inversion for source characterization of ridge-crest earthquakes (abstract), *Eos Trans. AGU*, **66**, 355, 1985.
- Bergman, E. A., J. L. Nabelek, and S. C. Solomon, An extensive region of off-ridge normal-faulting earthquakes in the southern Indian Ocean, *J. Geophys. Res.*, **89**, 2425–2443, 1984.
- Bungum, H., and E. S. Husebye, Seismicity of the Norwegian Sea: The Jan Mayen Fracture Zone, *Tectonophysics*, **40**, 351–360, 1977.
- Casey, J. F., J. F. Dewey, P. J. Fox, J. A. Karson, and E. Rosencrantz, Heterogeneous nature of oceanic crust and upper mantle: A perspective from the Bay of Islands Ophiolite complex, in *The Sea*, vol. 7, *The Oceanic Lithosphere*, edited by C. Emiliani, pp. 305–338, John Wiley, New York, 1981.
- Chapman, M. E., and S. C. Solomon, North American–Eurasian plate boundary in northeast Asia, *J. Geophys. Res.*, **81**, 921–930, 1976.
- Chen, W.-P., and P. Molnar, Focal depths of intracontinental and intraplate earthquakes and their implications for the thermal and mechanical properties of the lithosphere, *J. Geophys. Res.*, **88**, 4183–4214, 1983.
- Churkin, M., Jr., Western boundary of the North American continental plate in Asia, *Geol. Soc. Am. Bull.*, **83**, 1027–1036, 1972.
- Clowes, R. M., and S. Knize, Crustal structure from a marine seismic survey off the west coast of Canada, *Can. J. Earth Sci.*, **16**, 1265–1280, 1979.
- Cook, D. B., K. Fujita, and C. A. McMullen, Present-day plate interactions in northeast Asia: North American, Eurasian, and Okhotsk plates, *J. Geodyn.*, in press, 1986.
- Demenitskaya, R. M., and A. M. Karasik, The active rift system of the Arctic Ocean, *Tectonophysics*, **8**, 345–351, 1969.
- Duckworth, G. L., A. B. Baggeroer, and H. R. Jackson, Crustal structure measurements near FRAM II in the Pole Abyssal Plain, *Tectonophysics*, **89**, 173–215, 1982.
- Dziewonski, A. M., J. E. Franzen, and J. H. Woodhouse, Centroid-moment tensor solutions for April–June 1983, *Phys. Earth Planet. Inter.*, **33**, 243–249, 1983.

- Ebel, J. E., L. J. Burdick, and G. S. Stewart, The source mechanism of the August 7, 1966, El Golfo earthquake, *Bull. Seismol. Soc. Am.*, **68**, 1281–1291, 1978.
- Einsele, G., Basaltic sill-sediment complexes in young spreading centers: Genesis and significance, *Geology*, **13**, 249–252, 1985.
- Fuis, G. S., W. D. Mooney, J. H. Healy, G. A. McMechan, and W. J. Lutter, A seismic refraction survey of the Imperial Valley region, California, *J. Geophys. Res.*, **89**, 1165–1189, 1984.
- Fujita, K., D. B. Cook, H. Hasegawa, D. Forsyth, and R. Wetmiller, Seismicity and focal mechanisms of the Arctic and the North American plate boundary in Asia, in *The Decade of North American Geology*, vol. L, *The Arctic Ocean Region*, Geological Society of America, Boulder, Colo., in press, 1986.
- Grachev, A. F., Geodynamics of the transitional zone from the Moma Rift to the Gakkel Ridge, *Studies in Continental Margin Geology*, edited by J. S. Watkins and C. L. Drake, *Mem. Am. Assoc. Pet. Geol.*, **34**, 103–113, 1982.
- Grachev, A. F., and A. M. Karasik, Sea floor spreading and tectonics of the Eurasian basin (in Russian), Geotectonic Implications of the Prospects of Mineral Resources on the Arctic Shelf, *Tr. Nauchno Issled. Inst. Geol. Arktiki*, **19**–33, 1974.
- Grachev, A. F., R. M. Dement'skaya, and A. M. Karasik, The Mid-Arctic Ridge and its continental continuation (in Russian), *Geomorfologiya*, no. 1, 42–45, 1970.
- Hamilton, E. L., V_p/V_s and Poisson's ratios in marine sediments and rocks, *J. Acoust. Soc. Am.*, **66**, 1093–1101, 1979.
- Harper, G. D., Tectonics of slow spreading mid-ocean ridges and consequences of a variable depth to the brittle/ductile transition, *Tectonics*, **4**, 395–409, 1985.
- Huang, P. Y., Focal depths and mechanisms of mid-ocean ridge earthquakes from body waveform inversion, Ph.D. thesis, 301 pp., Mass. Inst. of Technol., Cambridge, 1985.
- Huang, P. Y., and S. C. Solomon, Centroid depths and mechanisms of mid-ocean ridge earthquakes in the Indian Ocean, Gulf of Aden, and Red Sea, *J. Geophys. Res.*, in press, 1986.
- Huang, P. Y., S. C. Solomon, E. A. Bergman, and J. L. Nabelek, Focal depths and mechanisms of Mid-Atlantic Ridge earthquakes from body waveform inversion, *J. Geophys. Res.*, **91**, 579–598, 1986.
- Hyndman, R. D., Poisson's ratio in the oceanic crust—A review, *Tectonophysics*, **59**, 321–333, 1979.
- Isacks, B., J. Oliver, and L. R. Sykes, Seismology and the new global tectonics, *J. Geophys. Res.*, **73**, 5855–5899, 1968.
- Jackson, H. R., I. Reid, and R. K. H. Falconer, Crustal structure near the Arctic mid-ocean ridge, *J. Geophys. Res.*, **87**, 1773–1783, 1982.
- Johnson, G. L., D. Monahan, G. Gronlie, and L. Sobczak, General bathymetric chart of the oceans (GEBCO), 5th ed., sheet 5.17, Can. Hydrogr. Serv., Ottawa, Ont., 1979.
- Karson, J. A., and H. J. B. Dick, Tectonics of ridge-transform intersections at the Kane Fracture Zone, *Mar. Geophys. Res.*, **6**, 51–98, 1983.
- Kogan, A. L., Seismic studies using CMRW and DSS from marine ice on the Arctic Sea shelf (exemplified by the Laptev Sea) (in Russian), Geophysical Surveys of the Arctic, no. 9, *Tr. Nauchno Issled. Inst. Geol. Arktiki*, 33–38, 1974.
- Kristoffersen, Y., The Nansen Ridge, Arctic Ocean: Some geophysical observations of the rift valley at slow spreading rate, *Tectonophysics*, **89**, 161–172, 1982.
- Kristoffersen, Y., E. S. Husebye, H. Bungum, and S. Gregersen, Seismic investigations of the Nansen Ridge during the FRAM I experiment, *Tectonophysics*, **82**, 57–68, 1982.
- Lachenbruch, A., J. H. Sass, and S. P. Galanis, Jr., Heat flow in southernmost California and the origin of the Salton Trough, *J. Geophys. Res.*, **90**, 6709–6736, 1985.
- Lister, C. R. B., Qualitative models of spreading-center processes, including hydrothermal penetration, *Tectonophysics*, **37**, 203–218, 1977.
- McKenzie, D., Some remarks on the development of sedimentary basins, *Earth Planet. Sci. Lett.*, **40**, 25–32, 1978.
- Minster, J. B., and T. H. Jordan, Present-day plate motions, *J. Geophys. Res.*, **83**, 5331–5354, 1978.
- Moore, D. G., Plate-edge deformation and crustal growth, Gulf of California structural province, *Geol. Soc. Am. Bull.*, **84**, 1883–1906, 1973.
- Nabelek, J. L., Determination of earthquake source parameters from inversion of body waves, Ph.D. thesis, 346 pp., Mass. Inst. of Technol., Cambridge, 1984.
- Nabelek, J. L., Geometry and mechanism of faulting of the 1980 El Asnam, Algeria, earthquake from inversion of teleseismic body waves and comparison with field observations, *J. Geophys. Res.*, **90**, 12,713–12,728, 1985.
- Nicolas, A., Novel type of crust produced during continental rifting, *Nature*, **315**, 112–115, 1985.
- Ostenso, N. A., Arctic Ocean margins, in *The Geology of Continental Margins*, edited by C. A. Burk and C. L. Drake, pp. 361–374, Springer-Verlag, New York, 1974.
- Pitman, W. C., III, and M. Talwani, Sea-floor spreading in the North Atlantic, *Geol. Soc. Am. Bull.*, **83**, 619–646, 1972.
- Poppe, B. B., D. A. Naab, and J. S. Perry, Seismograph station codes and characteristics, *U.S. Geol. Surv. Circ.* **791**, 171 pp., 1978.
- Rothé, J. P., *The Seismicity of the Earth*, 336 pp., UNESCO, Paris, 1969.
- Saunders, A. D., D. J. Fornari, and M. A. Morrison, The composition and emplacement of basaltic magmas produced during the development of continental margin basins: The Gulf of California, Mexico, *J. Geol. Soc. London*, **139**, 335–346, 1982.
- Savostin, L. A., and A. M. Karasik, Recent plate tectonics of the Arctic Basin and of northeastern Asia, *Tectonophysics*, **74**, 111–145, 1981.
- Shudofsky, G. N., Source mechanisms and focal depths of East African earthquakes using Rayleigh-wave inversion and body-wave modelling, *Geophys. J. R. Astron. Soc.*, **83**, 563–614, 1985.
- Solomon, S. C., and B. R. Julian, Seismic constraints on ocean-ridge mantle structure: Anomalous fault-plane solutions from first motions, *Geophys. J. R. Astron. Soc.*, **38**, 265–285, 1974.
- Sykes, L. R., The seismicity of the Arctic, *Bull. Seismol. Soc. Am.*, **55**, 501–518, 1965.
- Sykes, L. R., Mechanism of earthquakes and nature of faulting on the mid-ocean ridges, *J. Geophys. Res.*, **72**, 2131–2153, 1967.
- Sykes, L. R., Earthquake swarms and seafloor spreading, *J. Geophys. Res.*, **75**, 6598–6611, 1970.
- Tapponnier, P., and J. Francheteau, Necking of the lithosphere and the mechanics of slowly accreting plate boundaries, *J. Geophys. Res.*, **83**, 3955–3970, 1978.
- Tarr, A. C., New maps of polar seismicity, *Bull. Seismol. Soc. Am.*, **60**, 1745–1747, 1970.
- Trehu, A. M., J. L. Nabelek, and S. C. Solomon, Source characterization of two Reykjanes Ridge earthquakes: Surface waves and moment tensors; *P* waveforms and nonorthogonal nodal planes, *J. Geophys. Res.*, **86**, 1701–1724, 1981.
- Varga, R. J., and E. M. Moores, Spreading structure of the Troodos ophiolite, Cyprus, *Geology*, **13**, 846–850, 1985.
- Verosub, K. L., and E. M. Moores, Tectonic rotations in extensional regimes and their paleomagnetic consequences for oceanic basalts, *J. Geophys. Res.*, **86**, 6335–6349, 1981.
- Vogt, P. R., P. T. Taylor, L. C. Kovacs, and G. L. Johnson, Detailed aeromagnetic investigation of the Arctic Basin, *J. Geophys. Res.*, **84**, 1071–1089, 1979.
- Wetmiller, R. J., and D. A. Forsyth, Seismicity of the Arctic, 1908–1975, Arctic Geophysical Review, edited by J. F. Sweeney, *Publ. Earth Phys. Branch*, **45**(4), 15–24, 1978.
- Wyss, M., Apparent stresses of earthquakes on ridges compared to apparent stresses of earthquakes in trenches, *Geophys. J. R. Astron. Soc.*, **19**, 479–484, 1970.

E. A. Bergman and S. C. Solomon, Department of Earth, Atmospheric, and Planetary Sciences, Massachusetts Institute of Technology, Cambridge, MA 02139.

J. P. Jemsek, McLean Laboratory, Woods Hole Oceanographic Institution, Woods Hole, MA 02543.

J. L. Nabelek, Lamont-Doherty Geological Observatory of Columbia University, Palisades, NY 10964.

(Received April 7, 1986;
revised September 5, 1986;
accepted September 5, 1986.)